



Estimation of Three-Dimensional Boundary Layer Velocity Profiles on Swept Wings and Blended Wing Bodies

Kexin MA¹, Simon PRINCE¹

¹Centre for Aeronautics, Cranfield University, UK

Abstract

A rapid process of boundary layer (BL) velocity profile reconstruction is frequently required for wing surface drag estimation or for aircraft engine intake design. With the Viscous Full-Potential (VFP) method, accurate prediction of local boundary layer parameters can be provided with high speed. However, no information is given concerning velocity distribution within the boundary layer. Existing boundary layer reconstruction methods have been applied to five test cases of different freestream Mach number range, and comparisons have been carried out between their results and experimental velocity profiles. A new optimized method which can give reliable results for both the streamwise and the crossflow directions at different subsonic airspeed has then been developed. Comparisons have then been performed, for two of these test cases, between velocity profiles calculated using measured boundary layer parameters and VFP simulated ones. These results indicate that boundary layer velocity profiles calculated with the new method using boundary layer parameters computed by VFP simulations are reasonably accurate for a high aspect-ratio and medium (or small) sweep angle wing, at subsonic airspeed under suitable flow conditions. A VFP simulation followed by calculation using the new boundary layer reconstruction method can be a rapid process for the reconstruction of boundary layer profiles. This process has finally been demonstrated on a blended wing body for the reconstruction of velocity profiles on its upper surface, where the boundary layer could be ingested by an engine intake.

Keywords: Boundary Layer Profile; VFP; Blended Wing Body; Boundary Layer Ingestion

1. General Introduction

The blended wing body (BWB) concept represents a potential breakthrough in subsonic transport aircraft design. It has been shown in recent studies that a boundary layer ingestion (BLI) propulsion system can be applied on a BWB aircraft in order to gain better transport efficiency. A configuration with engines at the top of the trailing edge, on the surface or partially immersed into the body, would be an optimal design for a BWB aircraft [1]. The application of a BLI propulsion system can bring several benefits: a diminution of jet mixing loss due to the portion of reduced flow velocity ingested into the engine, and a reduction in airframe drag due to the decrease of wake mixing. However, with such a boundary layer ingestion propulsion system, a combination of low velocity boundary layer air and free stream air is ingested by the engines. This non-uniform ingested flow will cause engine performance loss and leads to higher fuel consumption [2], or even more serious issues like engine malfunctions. It is therefore important to be able to predict, relatively accurately and rapidly, the ingested boundary layer characteristics to allow the conceptual integration of a boundary layer ingesting propulsion system.

1.1 Role of VFP in boundary layer calculations

Viscous Full-Potential (VFP) is a high speed CFD (computational fluid dynamics) method first developed by ARA (Bedford) and RAE (Farnborough) [3]. It can be used to calculate the flow field around an isolated 3D-wing or a wing-body combination in a subsonic freestream. Shock wave effects are also captured in the simulation. Full details of the VFP method can be found in reference [21]. VFP simulations can be performed up to a Mach number of about 0.90. Local boundary layer parameters for swept wings can be provided with reasonable accuracy. The boundary layer parameters are obtained via the solution of the swept / tapered 3D boundary layer equations, which result in the

boundary layer displacement thickness δ^* , the streamwise boundary layer momentum thickness θ , the local friction coefficient c_f , the transformed boundary layer shape factor \bar{H} , and the direction change of the flow through the boundary layer β_w . Since the boundary layer equations are solved, the method does not output velocity profiles within the boundary layer. However, several theoretical reconstruction methods can be used to calculate boundary layer velocity profiles, using boundary layer parameters provided by VFP simulations. Thus, for a certain test case, a VFP simulation followed by a boundary layer velocity reconstruction can provide a rapid method for the estimation of boundary layer velocity profiles for design analysis. Boundary layers can be reconstructed along the whole wing surface in a short time.

The aim of this work is then to identify a general method which can reconstruct three-dimensional boundary layers on a swept wing or on a BWB aircraft with reasonable accuracy at different Mach numbers, using integral boundary layer parameters output from the VFP method.

2. Review of Previous Methods

It is assumed that on the wing area where the study will be carried out, the boundary layer is fully turbulent with no separations anywhere on the surface. A streamline coordinate system is used here [4]. As shown in *Figure 1*, a random streamline U_i within the boundary layer can be projected on to the body surface, and thus be decomposed into two flow components which are orthogonal mutually. One component is in the same direction as the freestream velocity vector, U_e . This is the streamline direction, and the distribution of velocity in this direction is represented by the curve u . The direction of the other component, which is also parallel to the surface but perpendicular to the streamwise direction, is defined as the crossflow direction. The crossflow velocity distribution is illustrated by the curve w . β_w is the angle between the wall streamline and the external streamline, and β is the angle between a random streamline within the boundary layer and the streamwise direction.

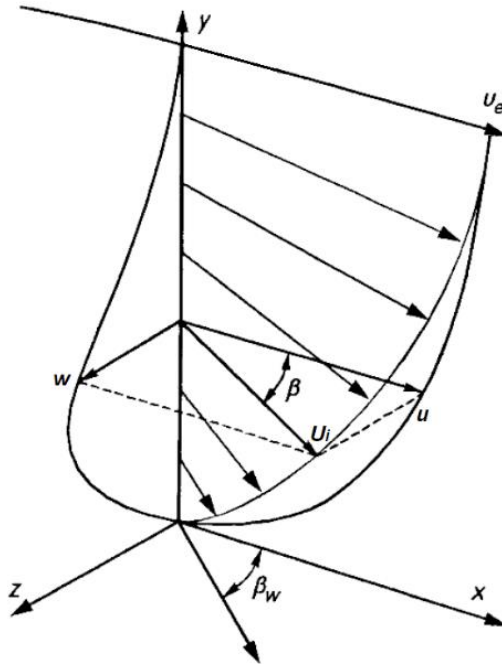


Figure 1 - Skewed velocity profile of a three-dimensional boundary layer within a streamline coordinate system [4].

2.1 The Streamwise Direction

It is assumed that the velocity distribution in the streamwise direction can be determined as that for a corresponding two-dimensional boundary layer [5]. Four methods have been published for the reconstruction of the streamwise component of the boundary layer velocity profile.

2.1.1 The Power law profile

It is mentioned in Reference [6] that, for an attached incompressible boundary layer, the velocity profile can be simply represented by a power law function:

$$\frac{u}{U_e} = \left(\frac{y}{\delta}\right)^{\frac{1}{n}} \quad (1)$$

where:

$$n = \frac{2}{H - 1} \quad (2)$$

The boundary layer thickness δ can be expressed in terms of n and the incompressible boundary layer momentum thickness θ_{inc} :

$$\frac{\delta}{\theta_{inc}} = \frac{(n + 1)(n + 2)}{n} \quad (3)$$

For incompressible flow the velocity profile can be expressed using power law profile as follows:

$$\frac{u}{U_e} = \left(\frac{n}{(n + 1)(n + 2)} \frac{y}{\theta_{inc}}\right)^{\frac{1}{n}} \quad (4)$$

For a compressible boundary layer, H and θ_{inc} in the previous equation should be replaced respectively by their corresponding transformed parameters \bar{H} and θ . These two parameters can be obtained directly from the VFP calculations. Otherwise, \bar{H} can be calculated by the following relation given in [7]:

$$\bar{H} = \frac{(H + 1)}{\left(1 + r \frac{\gamma - 1}{2} M_e^2\right)} - 1 \quad (5)$$

where $r = 0.9$ for a turbulent boundary layer [6], M_e is the Mach number at the top edge of the boundary layer and $\gamma = 1.4$ for air. Thus, for a compressible boundary layer:

$$n = \frac{2}{\bar{H} - 1} \quad (6)$$

and the velocity profile is:

$$\frac{u}{U_e} = \left(\frac{n}{(n + 1)(n + 2)} \frac{y}{\theta}\right)^{\frac{1}{n}} \quad (7)$$

2.1.2 Cole's profile

Coles' method [8] can be applied to a turbulent boundary layer on a smooth wall with an adverse mainstream pressure gradient. It is based on a combination of the law of the wall and the law of the wake, which can be shown by the following relationship:

$$\frac{u}{U_e} = 1 + \sigma A \log_{10} \frac{y}{\delta} - \left(2 - w\left(\frac{y}{\delta}\right)\right) \Pi(x) \quad (8)$$

with $\sigma = \sqrt{\frac{c_f}{2}}$ and A is a constant. Here w is the law of the wake and is represented as:

$$w\left(\frac{y}{\delta}\right) = 1 - \cos\left(\pi \frac{y}{\delta}\right) \quad (9)$$

The boundary layer velocity profile parameter $\Pi(x)$ can be calculated by resolving the following quadratic relationship:

$$\sigma W^2 \Pi^2(x) + \left[2\sigma \frac{A}{L} (2 + W_{log}) - \frac{H-1}{H}\right] \Pi(x) + \left[2\sigma \left(\frac{A}{L}\right)^2 - \frac{H-1}{H} \frac{A}{L}\right] = 0 \quad (10)$$

where W^2 and W_{log} are integrals defined from the law of the wake:

$$W^2 = \int_0^1 w^2\left(\frac{y}{\delta}\right) d\left(\frac{y}{\delta}\right) \quad (11)$$

$$W_{log} = \int_0^1 w^2\left(\frac{y}{\delta}\right) \ln\left(\frac{y}{\delta}\right) d\left(\frac{y}{\delta}\right)$$

The values of W^2 and W_{log} are calculated using eq. (11) and give $W^2 = 1.522$ and $W_{log} = -0.4$. $A = 5.8$ and $L = 2.3026$ as defined in Ref [9]. Thus, eq.(10) can be simplified to:

$$1.522\sigma \Pi^2(x) + \left[8.0605\sigma - \left(\frac{H-1}{H}\right)\right] \Pi(x) + \left[12.6896\sigma - 2.5189\left(\frac{H-1}{H}\right)\right] = 0 \quad (12)$$

It should be noticed that two values can be obtained by resolving eq.(12) and it is the larger value of the two that is used in the velocity profile relationship. The Coles' streamline velocity profile can then be expressed as follows:

$$\frac{u}{U_e} = 1 + \sqrt{\frac{c_f}{2}} \left[5.8 \log_{10} \left(\frac{y}{\delta} \right) - \left(1 + \cos \left(\pi \frac{y}{\delta} \right) \right) \Pi(x) \right] \quad (13)$$

For compressible flow, H should be replaced by its transformed form \bar{H} .

2.1.3 Lock's method

Lock suggested, for both attached and separated incompressible flows, the following equation to characterize boundary layer velocity profiles [6]:

$$\frac{u}{U_e} = \frac{u_\tau}{\kappa} \left[\ln \left(\frac{y}{\delta} u_\tau R e_\delta \right) + 2.13 \right] + C \sin^\chi \left(\frac{\pi y}{2 \delta} \right) \quad (14)$$

where $u_\tau = \pm \sqrt{\frac{1}{2} c_f}$, with a positive sign for attached flows and a negative if separation occurs. The parameter C is defined as follows in order to fulfill the boundary conditions:

$$C = 1 - \frac{u_\tau}{\kappa} [\ln(u_\tau R e_\delta) + 2.13] \quad (15)$$

χ is a parameter proposed by Cross [10] which describes the effect of boundary layer departure from equilibrium. Here the equilibrium state of a turbulent boundary layer means that its velocity profiles remain invariant in the streamwise direction.

$$\chi = 0.7 + 1.3e^{250\Pi} \quad (16)$$

with the departure from equilibrium Π defined as:

$$\Pi = \frac{\theta_{inc}}{U_e} \frac{dU_e}{dx} - \left(\frac{\theta_{inc}}{U_e} \frac{dU_e}{dx} \right)_{eq} \quad (17)$$

with $\left(\frac{\theta_{inc}}{U_e} \frac{dU_e}{dx} \right)_{eq}$ defined by Green as follows [7]:

$$\left(\frac{\theta_{inc}}{U_e} \frac{dU_e}{dx} \right)_{eq} = \frac{1.25}{H} \left[\frac{c_f}{2} - 0.0242 \left(\frac{H-1}{H} \right)^2 \right] \quad (18)$$

Therefore, Π and χ can be calculated using $\frac{\theta_{inc}}{U_e} \frac{dU_e}{dx}$, c_f and H obtained from VFP simulations. Boundary layer velocity profiles can then be calculated. For adiabatic compressible flows, Green suggested [7]:

$$\left(\frac{\theta}{U_e} \frac{dU_e}{dx} \right)_{eq} = \frac{1.25}{H} \left[\frac{c_f}{2} - \left(\frac{\bar{H}-1}{6.432\bar{H}} \right)^2 (1 + 0.04M_e^2)^{-1} \right] \quad (19)$$

and the eq.(17) should be written as:

$$\Pi = \frac{\theta}{U_e} \frac{dU_e}{dx} - \left(\frac{\theta}{U_e} \frac{dU_e}{dx} \right)_{eq} \quad (20)$$

2.1.4 Cross's method

In Ref [11] a method for three-dimensional compressible turbulent boundary layers was presented. This method was proposed by Cross [12]. The streamwise velocity profile is defined by:

$$\frac{u}{U_e} = \sqrt{\frac{c_f}{2}} \cos \beta_w \left[\frac{1}{\kappa} \ln \frac{y}{\delta} + b_s \left(\sin \chi_s \left(\frac{\pi y}{2 \delta} \right) - 1 \right) \right] + 1 \quad (21)$$

where:

$$b_n = -\frac{1}{\kappa} \ln \left(\sqrt{\frac{c_f}{2}} Re_\delta \right) - 5.0$$

$$b_s = b_n + \frac{\sqrt{2}}{\sqrt{c_f} \cos \beta_w}$$

$$\chi_s = \chi (1 - 0.1708 |\gamma_c|^{2.232})$$

$$\sin \gamma_c = \sin \beta_w \left[1 + 2 \sqrt{\frac{c_f}{2}} U_e b_n \cos \beta_w + \frac{c_f}{2} U_e^2 b_n^2 \right]^{\frac{1}{2}}$$

The parameter χ is the same as defined in eq.(16) and can be obtained using the method described in the previous section. Cross's method also includes a crossflow velocity profile, which will be explained in Section 2.2.3.

2.2 Crossflow Direction

For the prediction of crossflow velocity distribution of a three-dimensional turbulent boundary layer, three methods are available. Two of them are presented respectively by Mager [13] and Johnston [14]. And the last one is related to Cross's [12] streamwise velocity profile introduced in the previous subsection.

2.2.1 Mager's method

Mager suggested, for an incompressible turbulent boundary layer:

$$\frac{w}{U_e} = \frac{u}{U_e} \left(1 - \frac{y}{\delta} \right)^2 \tan \beta_w \quad (22)$$

where w is the crossflow velocity, u is the streamwise velocity and β_w the angle between the limiting wall streamline and the external streamline. For compressible flow, Smith [15] proposed that this relation might be generalized:

$$\frac{w}{U_e} = \frac{u}{U_e} \left(1 - \frac{Y}{Y_\delta} \right)^2 \tan \beta_w \quad (23)$$

where:

$$Y = \int_0^y \frac{\rho}{\rho_e} dy$$

$$Y_\delta = \int_0^\delta \frac{\rho}{\rho_e} dy$$

2.2.2 Johnston's method

Another model of crossflow velocity distribution was proposed by Johnston. It is validated for both incompressible and compressible flows. A sketch of this model is shown in Figure 2. As can be observed, the boundary layer is divided into two regions. In the Region I, which is near the wall:

$$\frac{w}{U_e} = \frac{u}{U_e} \tan \beta_w \quad (24)$$

and for the remaining part of the boundary layer Region II:

$$\frac{w}{U_e} = A \left(1 - \frac{u}{U_e} \right) \quad (25)$$

The parameter A is defined as follows:

$$A = \frac{\tan \beta_w}{0.1(c_{fx} \cos \beta_w)^{-1/2} - 1} \quad (26)$$

where c_{fx} the streamwise component of the local friction coefficient. It is related to the friction coefficient by:

$$c_{fx}(1 + \tan^2 \beta_w)^{1/2} = c_f \quad (27)$$

Johnston's profile still needs the x-coordinate of the junction point $(\frac{u}{U_e})_{int}$ of Region I and Region II:

$$\left(\frac{u}{U_e}\right)_{int} = \frac{1}{1 + \frac{\tan \beta_w}{A}} \quad (28)$$

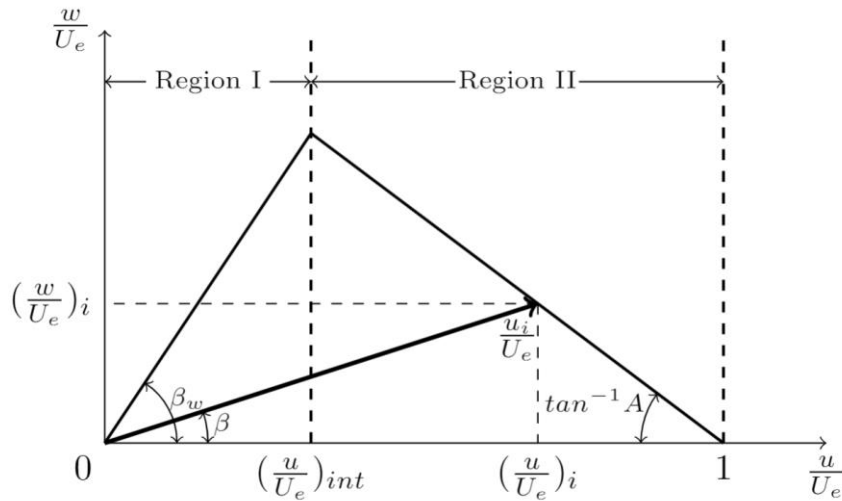


Figure 2 - Triangular model of Johnston

2.2.3 Cross's method

The crossflow velocity profile suggested by Cross [12] for a three-dimensional turbulent compressible boundary layer is given by the following relationship, where a part of the parameters are already defined when introducing the streamwise velocity profile in Section 2.1.4:

$$\frac{w}{U_e} = \sqrt{\frac{c_f}{2}} \sin \beta_w \left[\frac{1}{\kappa} \ln \frac{y}{\delta} + b_n \left(\sin \chi_n \left(\frac{\pi y}{2 \delta} \right) - 1 \right) \right] \quad (29)$$

with

$$\chi_n = \chi_s (1 - 0.4 \beta_w^2)$$

3. Prediction Method Validation

Five experimental data sets which cover different Mach number ranges have been used in order to evaluate the reliability of each prediction method.

3.1 M2155 Transonic Test Case

The first test case is Firmin and McDonald's experiment on the M2155 research wing [16]. This is a low-aspect-ratio wing ($AR = 3.27$), with a leading edge sweep angle of 39° and a trailing edge sweep angle of 15° . Detailed boundary layer measurements are provided in the data set for the purpose of validation of computational methods. This M2155 research wing has been designed deliberately so at different design conditions, different flow features can be exhibited. In some regions the boundary layer is subject to severe adverse pressure gradients, including some cases of separation. Forward shock waves appear on the upper surface, followed by a rear shock caused by shock sweep in the inboard region, thus form a triple-shock pattern.

3.1.1 Data analysis

The experiment was carried out under four different flow conditions in the Mach number range 0.6 to 0.87. For all the four test cases, boundary layer profiles have been studied at 11 different points on the upper surface of the wing, for the chord position x/c in the range of 0.40 to 0.85 and for the span position η (percentage along the wing span) from 0.24 to 0.80. In the streamwise direction, the four prediction methods introduced in the previous chapter have been used to obtain the velocity profiles thanks to boundary layer parameters provided at each measurement point. Regarding the prediction in the crossflow direction, the velocity distribution at each point has been calculated with Mager's and Johnston's methods, using respectively the Power Law profile and Coles' profile as the streamwise velocity profile, and also with Cross's method. Some typical examples of the boundary layer prediction will be shown and analyzed. One under flow conditions of a freestream Mach number $M_\infty = 0.744$ and an angle of incidence $\alpha = 2.5^\circ$, another under conditions of $M_\infty = 0.806$ and $\alpha = 2.5^\circ$.

Figure 3 shows an example of the trailing edge region's velocity profile at $M_\infty = 0.744$. For the streamwise velocity, the Power Law profile shows good agreement with the experimental data, with just a small underprediction in the region $\frac{y}{\delta} < 0.2$. Coles' profile fits very well with the measurement in this region, then tends to underestimate the velocity distribution above it. Lock's and Cross's methods give very similar results. They predict higher streamwise velocities than those measured in the near wall region ($\frac{y}{\delta} < 0.35$) and lower velocities in the middle region of the boundary layer ($0.35 < \frac{y}{\delta} < 0.8$). Only Mager's profiles give accurate prediction for the crossflow velocity, especially the one which uses Coles' profile in the streamwise direction. The other three methods predict excessive velocity in comparison to the measurement.

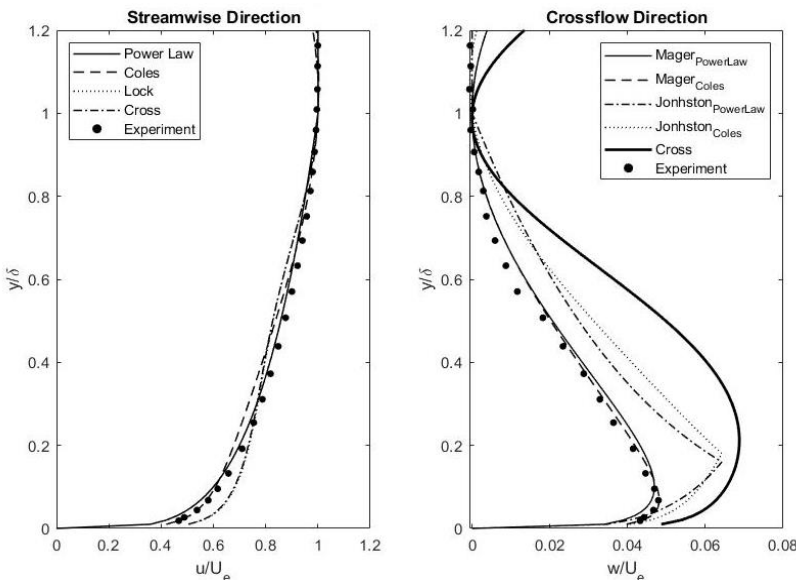


Figure 3 - Comparison of velocity profiles. M2155 wing. $M_\infty = 0.744$, $\alpha = 2.5^\circ$, $\eta = 0.494$, $x/c = 0.85$

Estimation of Three-Dimensional Boundary Layer Velocity Profiles on Swept Wings

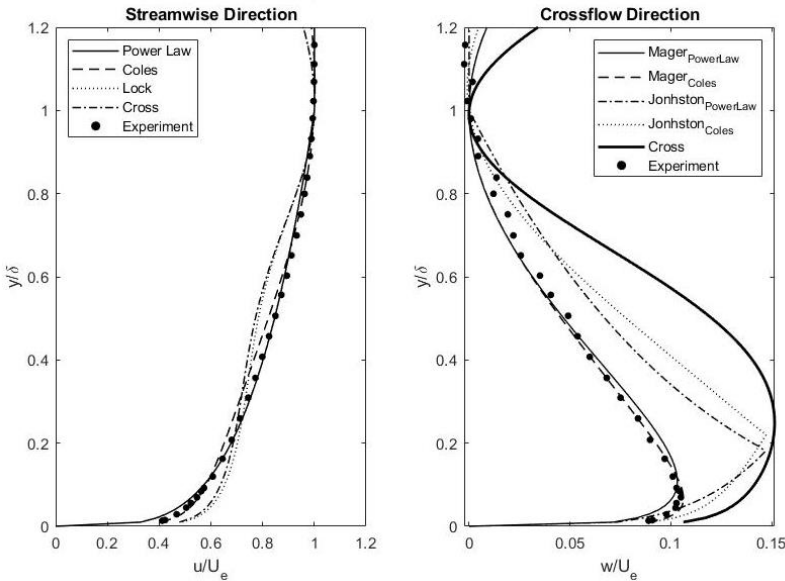


Figure 4 - Comparison of velocity profiles. M2155 wing. $M_\infty = 0.806$, $\alpha = 2.5^\circ$, $\eta = 0.299$, $x/c = 0.851$

Another example of the boundary layer profile inboard ($\eta = 0.3$) ahead of the leading edge ($x/c = 0.851$) is presented in figure 4. The two boundary profiles predicted by the Power Law and Coles' methods are quite close to the measurement: the Coles' profile fits better with the experimental data over the region from the wall to approximately $\frac{y}{\delta} = 0.1$ and over the region from around $\frac{y}{\delta} = 0.6$ to the edge of the boundary layer, while the Power Law profile agrees better with the measurement in the region between $\frac{y}{\delta} = 0.1$ and 0.6. These two $\frac{y}{\delta}$ values which differentiate prediction situations happen to be the two intersections of the Power Law profile and the Coles' profile. Concerning Lock's and Cross's methods, they have predicted velocity profiles closer to separation and much in error of the experimental result. The experimental crossflow profile fits really well with the Mager's profile using Coles' method for the streamwise profile. The one using a Power Law in the streamwise direction slightly overpredicts the crossflow profile over the region $0.2 < \frac{y}{\delta} < 0.4$, but underpredicts it close to the wall beneath this region. Both Johnston's profiles and Cross' profile largely overestimate the velocity distribution in the crossflow direction.

3.1.2 Optimization of the boundary layer reconstruction method

After having studied all boundary layer profiles available in this test, an optimized method which can provide better, more accurate prediction for all cases has been developed. It can be observed from previous boundary layer profile examples that, for the streamwise profile prediction, Lock's and Cross' methods do not always give good predictions. As for the Power Law and Coles' methods, they give closer prediction most of the time. For most situations, the profiles calculated by these two methods intersect two times. Coles' method gives better prediction from the wall to their first intersection, and from their second intersection up to the edge of the boundary layer. The Power Law profile is closer to the experimental results over the region between the two intersections.

With regard to the crossflow velocity profile, from a general point of view, Mager's profile using Coles' profile in the streamwise direction is the best choice. Indeed, Cross' and Johnston's profiles usually overpredict the crossflow velocity distribution, sometimes even a very high overprediction can be seen. For the boundary layer at a point on the upper surface of the wing where the integral parameters are known, the optimized method developed for this transonic test case is as follows:

- **Streamwise direction:** After having calculated the two intersections of the Power Law profile and the corresponding Coles' profile with Matlab (the intersection near the wall is named $(\frac{y}{\delta})_{first}$ and the one higher $(\frac{y}{\delta})_{second}$). The method then proposes the following profile:

Estimation of Three-Dimensional Boundary Layer Velocity Profiles on Swept Wings

$$\begin{aligned}
 u &= u_{Coles} & \text{for } & 0 < \frac{y}{\delta} \leq \left(\frac{y}{\delta}\right)_{first} \\
 u &= u_{PowerLaw} & \text{for } & \left(\frac{y}{\delta}\right)_{first} < \frac{y}{\delta} \leq \left(\frac{y}{\delta}\right)_{second} \\
 u &= u_{Coles} & \text{for } & \left(\frac{y}{\delta}\right)_{second} < \frac{y}{\delta} \leq 1 \\
 u &= U_e & \text{for } & 1 < \frac{y}{\delta}
 \end{aligned} \tag{30}$$

- Crossflow direction: It is proposed to reconstruct the crossflow profile as:

$$\begin{aligned}
 w &= w_{MagerColes} = u_{Coles} \left(1 - \frac{y}{\delta}\right)^2 \tan \beta_w & \text{for } & 0 < \frac{y}{\delta} \leq 1 \\
 w &= 0 & \text{for } & 1 < \frac{y}{\delta}
 \end{aligned} \tag{31}$$

The optimized method proposed here has been compared with measurements at different locations for M2155 transonic test case. Then comparisons have been made between the predicted boundary layer velocity profiles using this optimized method and the experimental data, for both streamwise and crossflow directions.

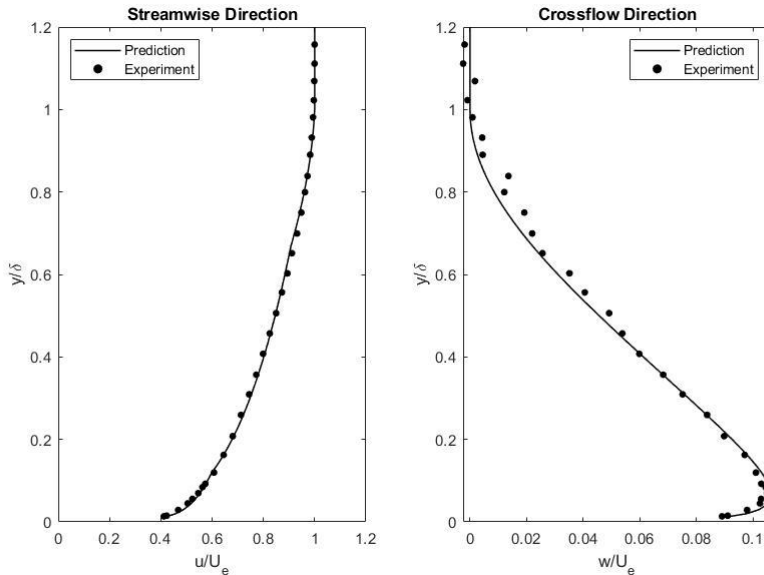


Figure 5 - Comparison of new optimised method result with experiment. M2155 wing. $M_\infty = 0.806$, $\alpha = 2.5^\circ$, $\eta = 0.299$, $x/c = 0.851$

The comparison of the optimized prediction profile and the experimental data is plotted in *Figure 5* and is based on the same case illustrated in *Figure 4*. The prediction point is located inboard ahead of the trailing edge of the wing. As explained formerly, the flow in this region is attached and the flow direction change is relatively small. The comparison shows that the prediction is quite accurate, especially in the streamwise direction. And this is the case for all the test points under these flow conditions (where neither separation nor high boundary layer skewness exists).

3.2 RAE101 Subsonic Test Case

This experiment [17] was carried out on a quasi-infinite swept wing of RAE 101 section at two different

Estimation of Three-Dimensional Boundary Layer Velocity Profiles on Swept Wings

freestream Mach number (one around 0.7 and the other around 0.4), at sweep angles of 20° and 28° . Static pressure distributions were measured on both the upper and the lower surfaces of the wing, and also through the wake. Boundary layer integral parameters as well as boundary layer velocity profiles are provided in the data set, at a position near the leading edge ($x/c=0.280$) and at several positions in the trailing edge region on the upper surface. As having been done for the M2155 transonic test case, different prediction methods have been applied at the measuring points, then comparisons have been carried out for each measuring point between predicted profiles and the experimental ones.

Figure 6 shows the comparison between the different reconstruction methods and the measurement at sweep angle of 20° , at an angle of incidence of 0° and at a freestream Mach number of 0.426. It can be observed that in the streamwise direction, both the Power Law and Coles' methods give similar results compared to the experimental profile. In the near-wall region ($0 < \frac{y}{\delta} < 0.1$) and in the near-stream region ($0.6 < \frac{y}{\delta} < 1$), Coles' profile is slightly closer to the measurement than the Power Law profile. While it is the contrary situation in the middle region ($0.1 < \frac{y}{\delta} < 0.6$). The experimental crossflow velocity profile, as can be observed in the same figure, is not smooth in the middle region of the boundary layer. This is maybe due to limitations in measurement accuracy. None of the predicted crossflow profiles fits well with the experimental one. Among them, the Cross' method largely overpredicts the velocity profile. The Mager's and Johnston's methods provide closer predictions with the measurement compared to Cross'. The former underpredicts the velocity profile and is more accurate in the near-wall region, while the latter overpredicts it and gives better results in the upper region. Of the two, the Mager's method is a little bit more accurate from a general point of view.

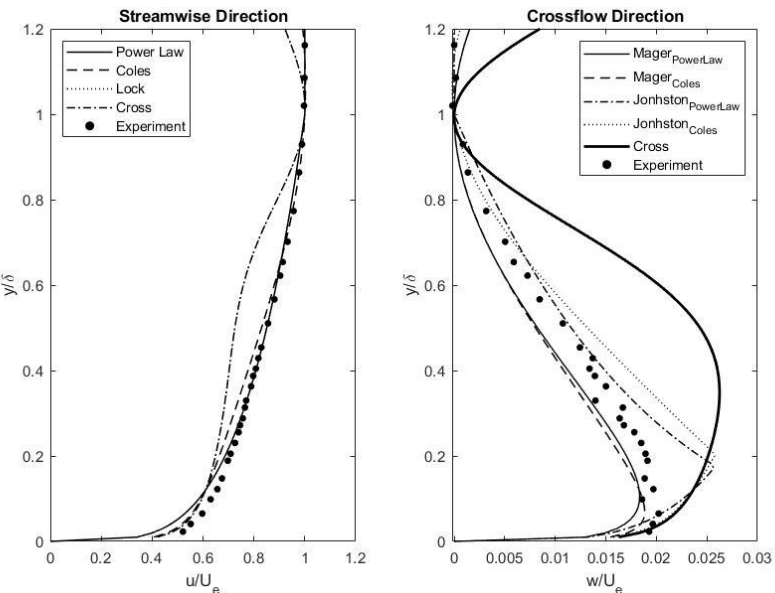


Figure 6 - Comparison of velocity profiles. RAE101 20° swept wing. $M_\infty = 0.426$, $\alpha = 0^\circ$, $x/c = 0.814$

The optimized method is thus applied to each measuring point of the RAE101 test case. An example result is shown in *Figure 7*. It can be observed that the optimized profile fits relatively well with the experimental data, in both streamwise and crossflow directions. The optimized function gives a small underprediction of approximately 5% for the streamwise velocity profile over the region ($0 < \frac{y}{\delta} < 0.2$). However, it is accurate over the rest of the boundary layer. In the crossflow direction, the optimized method provides a velocity profile which has $\frac{w}{U_e}$ values around 0.002 smaller than the experimental ones at the same $\frac{y}{\delta}$. This difference is small enough so that the crossflow velocity profile estimation can be considered acceptable.

For most cases of the RAE101 experimental data set, the optimized method is capable to give accurate prediction in the streamwise direction. With respect to the velocity profile in the crossflow direction, the optimized method always provides small underprediction compared to the experimental profile. But in general, this optimized method is able to provide acceptably accurate boundary layer profile predictions for design purpose.

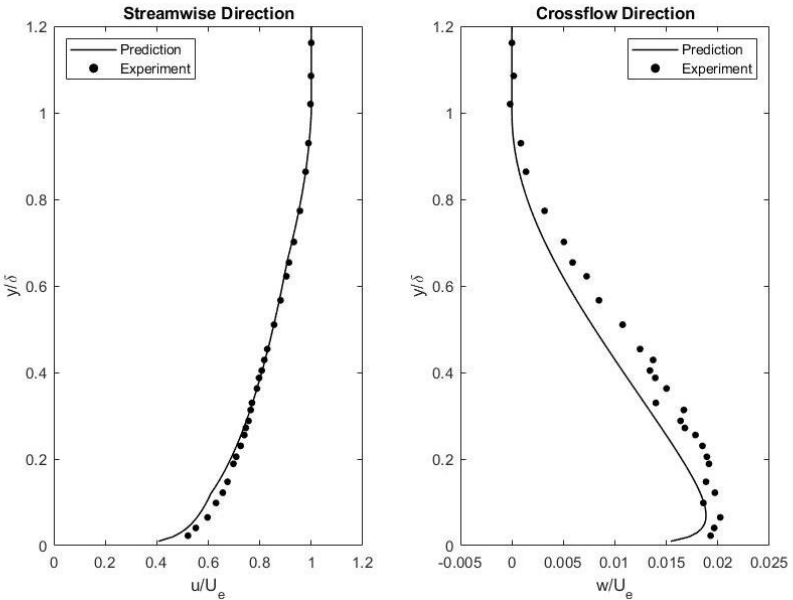


Figure 7 - Comparison of new optimised method result with experiment. M2155 wing. $M_\infty = 0.426$, $\alpha = 0^\circ$, $x/c = 0.814$

3.3 Berg and Elsenaar's Low Speed Test Case

Berg and Elsenaar's experiment [18] was carried out on an infinite flat plate at constant low freestream air speed (35m/s) in an adverse pressure gradient. The experiment was designed attentively so that the flow condition was very similar to that of an infinite swept wing. Three-dimensional boundary layer profiles were measured at ten points along the line parallel to the leading edge at 50% spanwise position, from $x/c = 0.33$ to $x/c = 0.89$. In this measuring range, the boundary layer develops progressively from a nearly two-dimensional boundary layer, to a three-dimensional one, then finally to a boundary layer separation.

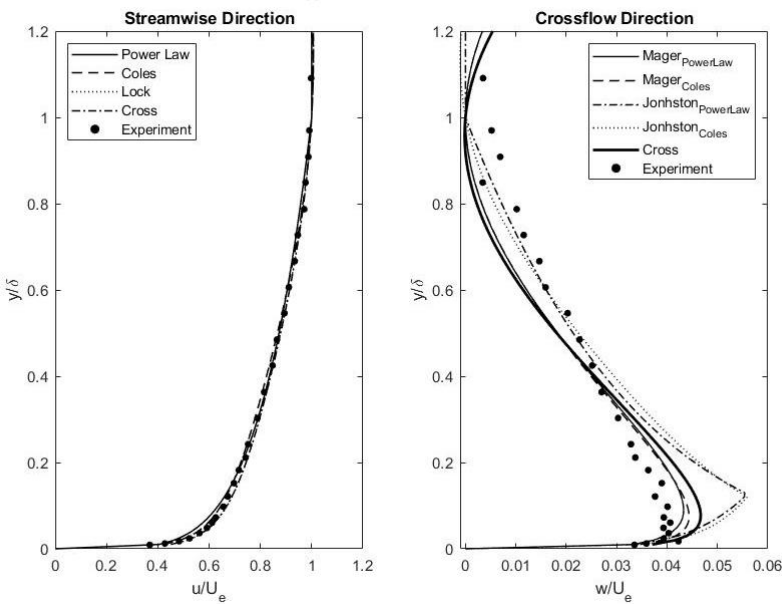


Figure 8 - Comparison of velocity profiles. Berg & Elsenaar experiment. $M_\infty = 0.103$, $x/c = 0.45$

Figure 8 illustrates the velocity profile in the middle region on the wing. It can be observed that in the crossflow direction, all the prediction methods over-predict the velocity distribution in the near-wall region ($y/\delta < 0.4$) but under-predict it in the near-stream region ($0.4 < y/\delta < 1$). While in the streamwise direction, all the predicted profiles are quite similar and all of them match well with the experimental data.

Estimation of Three-Dimensional Boundary Layer Velocity Profiles on Swept Wings

The optimized method was applied to all the measurement points as for other test cases. Figure 9 shows that the optimized function gives very accurate prediction in the streamwise direction. In regard to the crossflow direction, there are small differences, but the predicted profile agrees globally well with the measured one, and the accuracy is acceptable for conceptual design purposes.

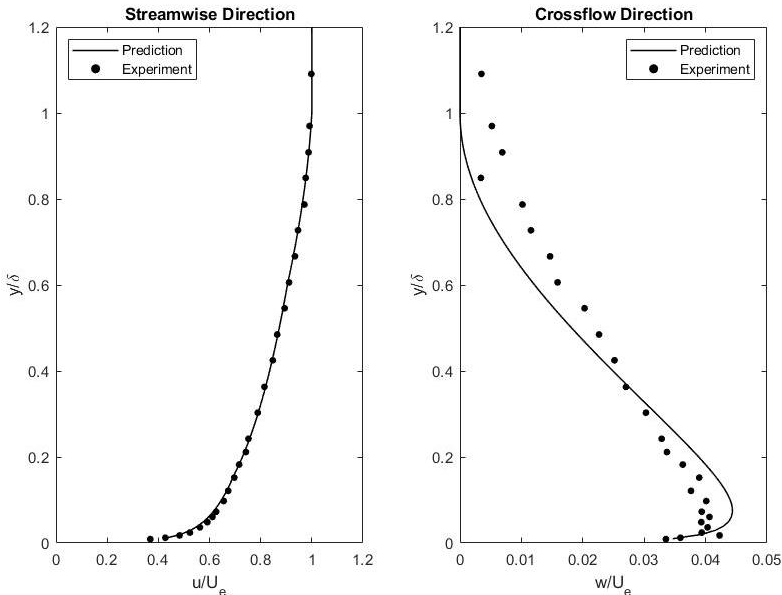


Figure 9 - Comparison of new optimised method result with experiment. Berg & Elsenaar Experiment.
 $M_\infty = 0.103$, $x/c = 0.45$

3.4 Supersonic Test Cases

Two supersonic experimental data sets were selected from Reference [19]. Both were conducted on flat plates with no flow heat transfer, one over the Mach number range 2.2-2.5 and the other around $M=4$. Boundary layer integral parameters were published in both data sets. Unfortunately, velocity profiles were only measured in the streamwise direction so only streamwise profile prediction was analysed in this study. Predicted profiles were compared with experimental ones at different measurement points and under various flow conditions. An example is illustrated in Figure 10. It can be observed that very large excursions can be seen between the predicted velocity profiles, and those measured in experiment. This is typical of the results for all of the supersonic and hypersonic cases investigated.

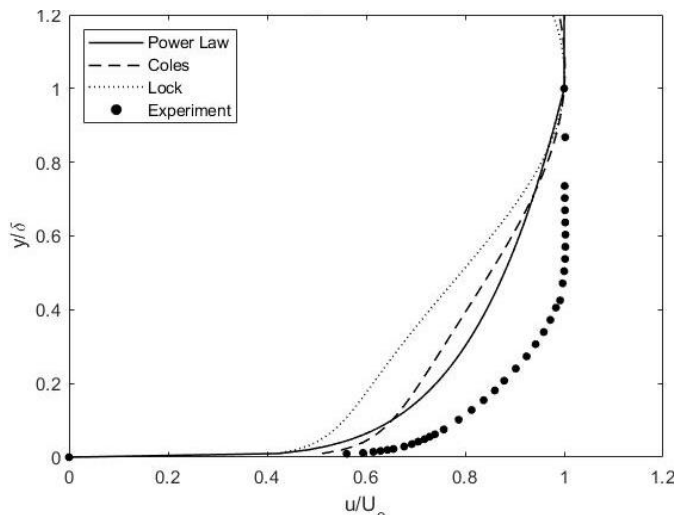


Figure 10 – A typical velocity profile prediction for a supersonic test case. Hastings & Sawyer flat plate case. $M = 4$, $x = 0.400$.

The inaccuracy appeared in predictions for supersonic test cases is due to the fact that all the

theoretical prediction methods work based on one hypothesis: pressure, temperature and density within the boundary layer are all constant. This is, indeed, practically correct for subsonic Mach numbers, and the change of these properties can be considered negligible in transonic cases. At very high Mach number ($M > 2$), however, the pressure, temperature and density variations within the boundary layer must be taken into account.

4. Validation of VFP Results with Experiments

VFP is able to calculate wing pressure distributions, local boundary layer parameters along the wing surface and a summary of the local and total forces and moments within a few minutes, with an accuracy approaching that of RANS predictions for attached flow cases. Simulations have been carried out for the M2155 wing and the RAE101 wing, under the same flow conditions in the experiments. Velocity profiles are calculated using, respectively, boundary layer parameters provided in the experimental data set and from VFP results.

4.1 M2155 Test Case

Figure 11 shows an example of the boundary layer profile at a measuring point inboard ($\eta = 0.24$) at $x/c = 0.441$, under the flow condition of $M_\infty = 0.806$. In the streamwise direction, the velocity profile predicted using experimental boundary layer parameters and the one calculated with VFP boundary layer parameters overlap. Both show very good agreement with the experimental velocity profile. As for the crossflow velocity profile, the two provide results with reasonable accuracy compared to the measured velocity profile, where the method using experiment parameters gives better agreement in the lower portion of the boundary layer below $y/d = 0.2$, but less accurate above this height.

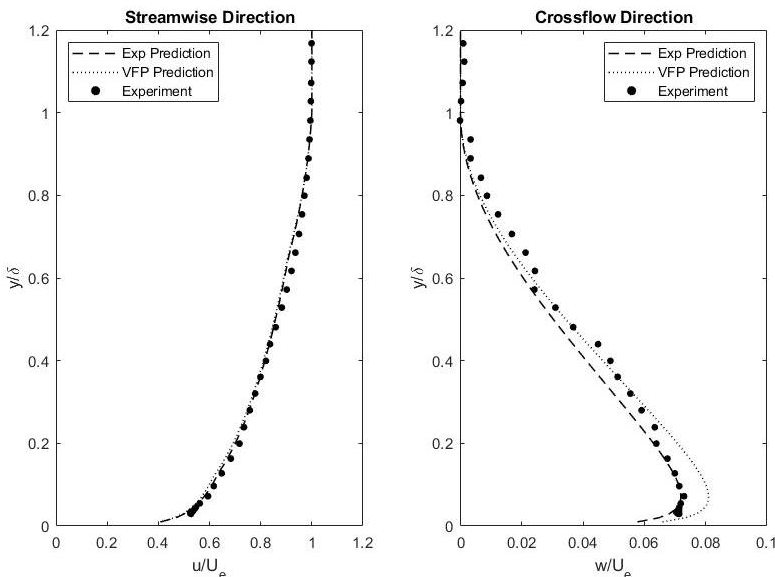


Figure 11 - Comparison of boundary layer velocity profiles: new method (using experimentally derived and VFP predicted boundary layer parameters) versus experiment for the M2155 wing.

$$M_\infty = 0.806, \alpha = 2.5^\circ, \eta = 0.238, x/c = 0.441$$

Another example is illustrated by Figure 12. The measuring point is located in the outboard region of the wing ($\eta = 0.77$) and the freestream Mach number $M_\infty = 0.854$. At this point, differences between boundary layer parameters provided VFP simulation and experimental data are relatively big. It can be observed that the predicted profile is very different from the one using measured boundary layer parameters. The latter shows good accuracy compared to the experimental profile while the agreement for the former is very poor. Especially for the crossflow velocity profile, the measurement shows that the velocity is negative in the near-wall region. However, the velocity profile calculated with VFP boundary layer parameters is completely positive. This is mainly due to the fact that this measuring point is close to the shock, VFP predicts very different boundary layer skewness angle value (38°) from the measurement (-1°), which is associated with the proximity of the shock wave. While the VFP

predicted boundary layer profiles are as accurate as those shown in figure 11 over 90% of the measurement stations assessed, those in regions, like this, close to the shock wave and also those at the wing tip where very strong spanwise flows develop, can be considerably in error of the experimental measurements.

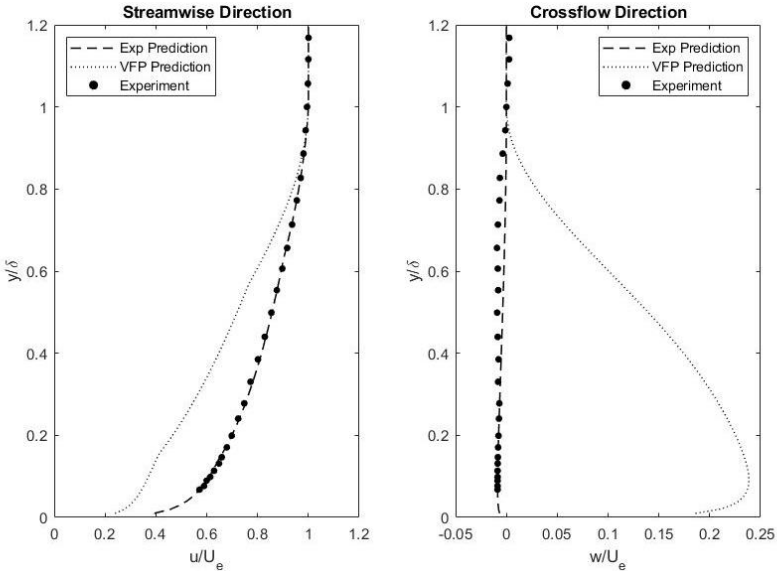


Figure 12 - Comparison of boundary layer velocity profiles: new method (using experimentally derived and VFP predicted boundary layer parameters) versus experiment for the M2155 wing.

$$M_\infty = 0.854, \alpha = 1.5^\circ, \eta = 0.771, x/c = 0.402$$

4.2 RAE101 Test Case

Figure 13 shows an example at a measuring point ($M_\infty = 0.718, \alpha = 1.88^\circ$ and $x/c = 0.814$) of the 20° swept RAE101 experiment. At this point, the VFP prediction of local skin friction coefficient is slightly higher than the experimental data. But other three boundary layer parameters are calculated quite accurately. It can be observed that the velocity profile calculated with VFP boundary layer parameters is slightly higher than that calculated with experimental parameters, in both directions. The maximum difference between these two profiles is about 15% in the streamwise direction and 12% in the crossflow direction. Comparing with the measured profiles, the experimental predicted profile agrees better in the streamwise direction. As for in the crossflow direction, none of these two profiles fits really well with the measured one, but both of them can provide reasonably accurate result for the purposes of rapid conceptual design.

VFP simulation can give reasonably accurate results of boundary layer parameters for a high aspect ratio wing at medium sweep angle, and at subsonic or transonic freestream air speed. The optimized prediction method for boundary layer velocity profiles can be applied to this type of wing, using boundary layer parameters computed by VFP. Results obtained show good agreement with measured velocity profiles, except in regions close to a shock and close to the tip of the wing. With respect to low aspect ratio or high sweep angle wings at high freestream Mach number, VFP can only predict accurately in the regions where the flow remains steady. It is not able to give good results near strong shock regions, where flow separation approaches or occurs, and where the flow direction change is important (where the boundary layer is highly three-dimensional). When using the optimized method, the prediction of boundary layer profiles are quite accurate at steady flow locations, in both streamwise and crossflow directions. However, the prediction can be totally aberrant at points located in unsteady flow regions.

Estimation of Three-Dimensional Boundary Layer Velocity Profiles on Swept Wings

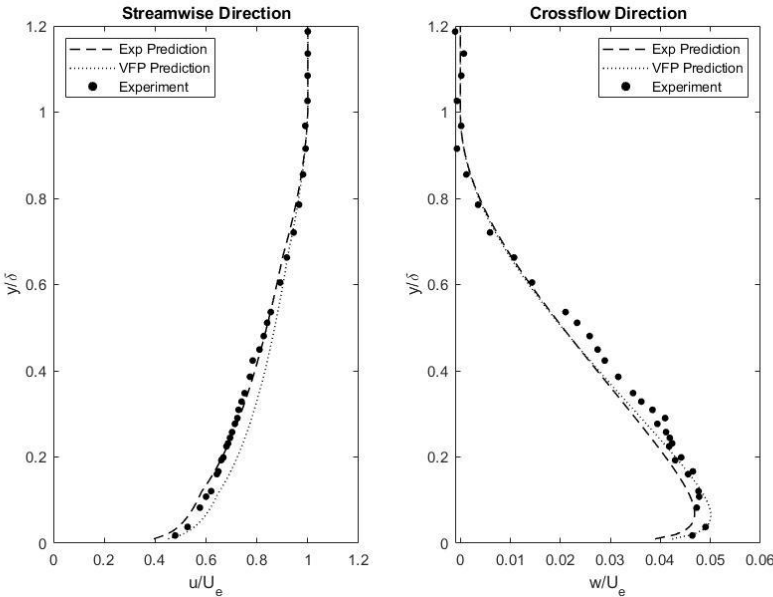


Figure 13 - Comparison of boundary layer velocity profiles: new method (using experimentally derived and VFP predicted boundary layer parameters) versus experiment for the 20° swept RAE101 wing. $M_\infty = 0.718$, $\alpha = 1.88^\circ$, $x/c = 0.814$.

5. Application of Validated Method to BWB

VFP was used to predict the transonic flow about the Cranfield BW-11 blended wing body configuration that was developed for theoretical design-analysis at Cranfield University. Full details of this configuration can be found in references [20] and [21]. VFP simulations of the BWB have been carried out at a fixed freestream Mach number $M_\infty = 0.80$ and at a fixed Reynolds number of 7.4×10^8 . Data was obtained at angle of incidence from 0° to 2.25° , with an increment of 0.25° . Details of the calculations are provided in reference [21]. The boundary layer was considered two-dimensional in this study and the velocity profile predictions were carried out only in the streamwise direction. The optimized streamwise velocity prediction method introduced previously has been applied to 4 locations along the local chord ($x/c = 0.50, 0.60, 0.70$ and 0.80), which belong to respectively 6 different span locations from inboard at $\eta = 0.3$ to outboard at $\eta = 0.80$ with an interval of 0.1 and at the centerline of the BWB ($\eta = 0.01$). The pressure distributions and the boundary layer shape factor distribution along the blended wing body at these span locations have been studied as well, for the purpose of analyzing flow conditions.

Figure 14 and Figure 15 show respectively the pressure distribution and the shape factor distribution outboard at $\eta = 0.8$ of the BWB. It can be observed that a weak shock is formed on the upper surface in the leading edge region. And the boundary layer shape factor distribution shows that a peak occurs around $x/c = 0.2$, which is just behind the shock. The values of \bar{H} achieve 2.3 here, which means that boundary layer separation approaches in this area. But from the mid-chord to 80% of the chord, no significant pressure change can be observed. Apart from this, it can be observed that \bar{H} values over this interval are around 1.5. The flow condition fulfills the working hypothesis of VFP over this interval. The boundary layer parameters provided by VFP simulation should be reliable in this case. The optimized prediction method is able to give accurate results as well. The boundary layer velocity profiles obtained are presented in Figure 16.

Estimation of Three-Dimensional Boundary Layer Velocity Profiles on Swept Wings

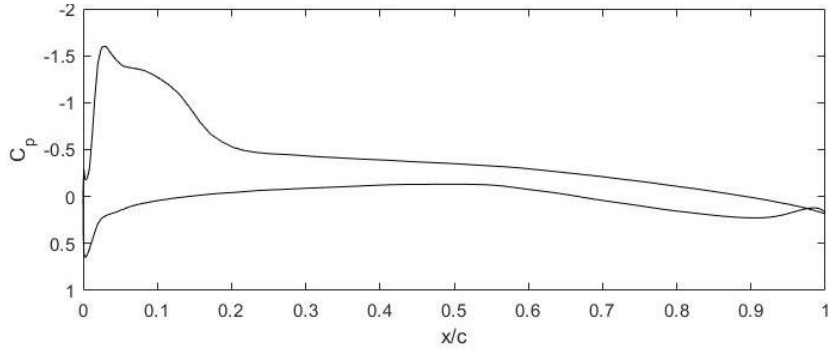


Figure 14 - BWB pressure distribution. $M_\infty = 0.80$, $\alpha = 2.25^\circ$ $\eta = 0.8$

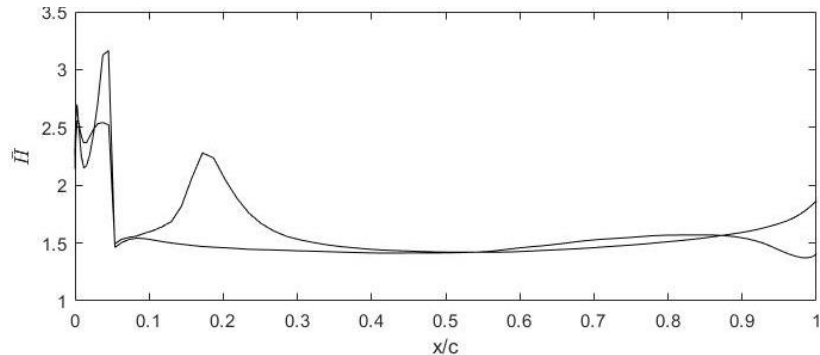


Figure 15 - BWB shape factor distribution. $M_\infty = 0.80$, $\alpha = 2.25^\circ$ $\eta = 0.8$

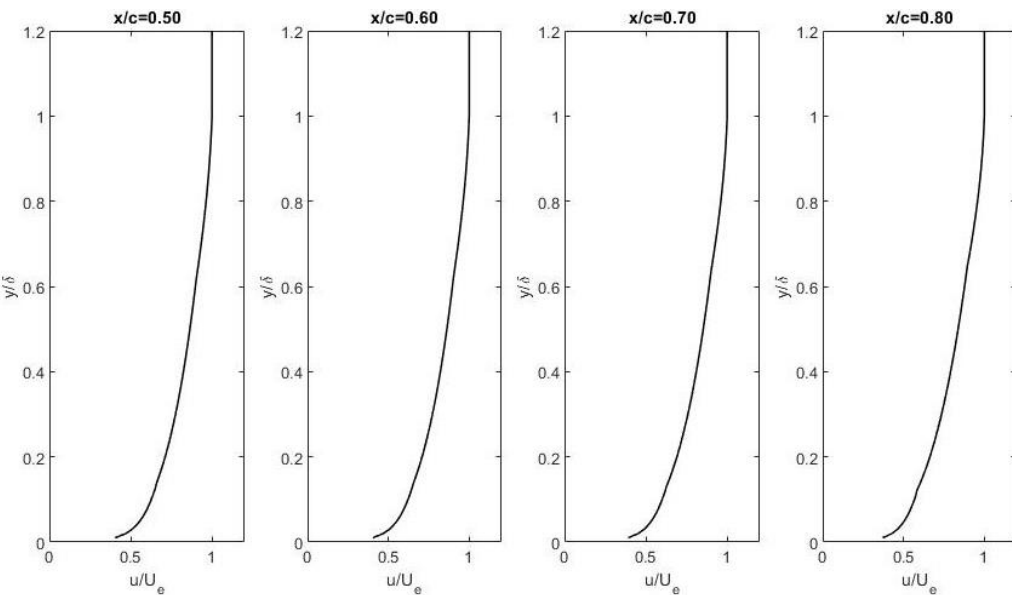


Figure 16 - Example of BWB upper surface boundary layer profiles. $M_\infty = 0.80$, $\alpha = 2.25^\circ$ $\eta = 0.8$

6. Conclusions

This study aimed to find out the most appropriate rapid process for the reconstruction of the three-dimensional boundary layer velocity profiles on a swept wing or on a blended-wing-body aircraft. Comparisons have been carried out between different existing theoretical prediction methods and experimental data for 5 different test cases, which cover freestream Mach number range from 0.1 to 4. The VFP (Viscous Full-Potential) method is capable of providing reasonably accurate boundary layer parameters under steady, irrotational and isentropic flow conditions for velocity profile predictions.

At subsonic airspeed, the prediction method which blends the Power Law and Coles' methods is able

to give better results in the streamwise direction compared to all other existing theoretical methods, and tends to fit well with experimental data for most test cases. The Mager's profile using Coles' profile as the streamwise velocity profile can provide acceptable predictions but not as accurate as the optimized method for streamwise velocity profile predictions. The application of VFP simulation followed by calculations with the optimized prediction method to a BWB aircraft has demonstrated that the boundary layer profiles on its upper surface can be reconstructed rapidly.

This study contributes to an improvement of simulation speed and accuracy of boundary layer velocity profiles on a swept wing or a blended-wing-body. The results obtained can be served in rapid and accurate drag estimation caused by surface imperfections, also in aircraft intake design and analysis.

7. Copyright Statement

The authors confirm that they, and/or their company or organization, hold copyright on all of the original material included in this paper. The authors also confirm that they have obtained permission, from the copyright holder of any third party material included in this paper, to publish it as part of their paper. The authors confirm that they give permission or have obtained permission from the copyright holder of this paper, for the publication and distribution of this paper as part of the ICAS proceedings or as individual off-prints from the proceedings.

References

- [1] H. J. M. Kok, M. Voskuijl and M. J. L. v. Tooren, "Distributed propulsion featuring boundary layer ingestion engines for the blended wing body subsonic transport," AIAA Paper 2010-3064.
- [2] D. Hall, A. Huang, A. Uranga, E. Greitzer, M. Drela & S. Sato, "Boundary layer ingestion propulsion benefit for transport aircraft," *Journal of Propulsion and Power*, vol. 33, no. 5, pp. 1118-1129, 2017.
- [3] K. C. Hackett and D. R. Philpott, "Visous full-potential (VFP) method for three-dimensional wings and wing-body combinations," ESDU Item 13012, 2014.
- [4] H. Schlichting and K. Gersten, *Boundary Layer Theory*, Berlin: Springer, 2017.
- [5] P. D. Smith, "An integral prediction method for three-dimensional compressible turbulent boundary layers," ARC R. & M. No. 3739 , 1972.
- [6] K. C. Hackett, "An assessment of methods for estimation of turbulent boundary-layer profiles (Unpublished)," ESDU, 2017.
- [7] J. E. Green, D. J. Weeks and J. W. F. Broome, "Prediction of turbulent boundary layers and wakes in compressible flow by a lag-entrainment method," ARC R.&M.No.3791, 1977.
- [8] D. Coles, "The law of the wake in the turbulent boundary layer," *Journal of Fluid Mechanics*, vol. 1, no. 2, pp. 191-226, 1956.
- [9] E. L. Houghton and R. P. Boswell, *Further Aerodynamics for Engineering Students*, London: Edward Arnold, 1969.
- [10] A. G. T. Cross, "Two-dimensional boundary layer calculations using a three parameter velocity profile," British Aerospace , Brough , 1980.
- [11] D. A. Humphreys and J. P. F. Lindhout, "Calculation methods for three-dimensional turbulent boundary layers," *Progress in Aerospace Science*, no. 25, pp. 107-129, 1988.
- [12] A. G. T. Cross, "Calculation of compressible three-dimensional turbulent boundary layers with particular reference to wings and bodies," British Aerospace, Brough, 1979.
- [13] A. Mager, "Generalization of boundary layer momentum integral equations to three-dimensional flows, including those of rotating systems," NACA Report 1067, 1952.
- [14] J. P. Johnston, "On the three-dimensional turbulent boundary layer generated by secondary flow," *Journal of Basic Engineering* , no. 82, pp. 233-250, 1960.
- [15] P. D. Smith, "An integral prediction method for three-dimensional compressible turbulent boundary layers," ARC R. & M. No. 3739, 1972.
- [16] M. C. P. Firmin and M. A. McDonald, "Measurements of the flow over a low aspect ratio wing in the mach number range 0.6 to 0.87 for the purpose of validation of computational methods," DRA Technical Report 92016., 1992.

Estimation of Three-Dimensional Boundary Layer Velocity Profiles on Swept Wings

- [17] P. H. Cook, M. A. McDonald and M. C. P. Firmin, "Wind tunnel measurements of the mean flow in the turbulent boundary layer and wake in the region of the trailing edge of a swept wing at subsonic speeds," RAE TR 79062, 1979.
- [18] B. van den Berg and A. Elsenaar, "Measurements in a three-dimensional incompressible turbulent boundary layer in an adverse pressure gradient under infinite swept wing condition," NLR Tech. Rep. no. 72092 U., 1972.
- [19] H. H. Fernholz and P. J. Finley, "A critical compilation of compressible turbulent boundary layer data," AGARD AG-223, 1977.
- [20] P. P. C. Okonkwo, "Conceptual Design Methodology for Blended Wing Body Aircraft," Cranfield University, PhD Thesis, 2016.
- [21] S. A. Prince, D. Di Pasquale and K. P. Garry, "Progress towards a rapid method for conceptual aerodynamic design for transonic cruise," in *AIAA Paper 2020-1286*, 2020.